Approach to the metal-insulator transition in $La_{1-x}Ca_xMnO_3$ $(0 \leqslant x \leqslant 0.2)$: Magnetic inhomogeneity and spin-wave anomaly

G. Biotteau,[1] M. Hennion,[1] F. Moussa,[1] J. Rodríguez-Carvajal,[1] L. Pinsard,[2] A. Revcolevschi,[2] Y. M. Mukovskii,[3] and D. Shulyatev[3]

[1]*Laboratoire Léon Brillouin, CEA-CNRS, CE Saclay, 91191 Gif sur Yvette Cedex, France*

[2]*Laboratoire de Physico-Chimie de l'Etat Solide, Université Paris-Sud, 91405 Orsay Cedex, France*

[3]*Moscow State Steel and Alloys Institute, Leninskii Prospect 4, Moscow 117936, Russia*

(Received 25 January 2001; published 23 August 2001)

We describe the evolution of the static and dynamic spin correlations of $La_{1-x}Ca_xMnO_3$ for $x=0.1$, 0.125, and 0.2, where the system evolves from the canted magnetic state towards the insulating ferromagnetic state, approaching the metallic transition ($x=0.22$). In the $x=0.1$ sample, the observation of two spin-wave branches typical of two distinct types of magnetic coupling and of a modulation in the elastic diffuse-scattering characteristic of ferromagnetic inhomogeneities confirms the static and dynamic inhomogeneous features previously observed at $x<0.1$. The anisotropic q dependence of the intensity of the low-energy spin wave suggests a bidimensional character for the static inhomogeneities. At $x=0.125$, which corresponds to the occurrence of a ferromagnetic and insulating state, one spin wave branch, anisotropic, is detected. At this concentration, an anomaly appears at $\mathbf{q}_0=(1.25, 1.25, 0)$. At $x=0.2$, the spin-wave branch appears as isotropic. In addition to the anomaly observed at q_0, extra magnetic excitations are observed at larger q, forming an optical branch.

DOI: 10.1103/PhysRevB.64.104421 PACS number(s): 75.30.Kz, 61.12.−q

I. INTRODUCTION

The doped rare-earth manganites have now been studied for several decades.[1,2] They have raised a renewed interest because of their colossal magnetoresistance observed beyond a critical value of doping rate. However, the physics driving these properties are still unclear. At low doping, the nature of the magnetic ground state is still a well-debated issue. From a theoretical point of view, depending on parameter values, the fundamental state can be either a homogeneous canted antiferromagnetic state[3,4] or an inhomogeneous state with a phase separation between hole-rich (Mn^{4+}) ferromagnetic regions and hole-poor (Mn^{3+}) antiferromagnetic domains.[4–9] At higher concentrations, the existence of a ferromagnetic and insulating phase is also very intriguing. It stresses out that the double-exchange coupling alone, which predicts a ferromagnetic and metallic state, is insufficient to explain the magnetic properties.[10,11] Around a doping rate of $x=0.125$, several works on the Sr-doped compounds have reported anomalous structural and magnetic properties at low temperature,[12,13] interpreted in terms of an orbital ordering[14] in these systems. A comparison with Ca substitution is needed for a deeper understanding of these effects.

Neutron scattering is a very powerful technique to describe, at an atomic scale, the evolution of a magnetic system from an insulating state to a metallic one. In previous papers devoted to the $x=0$, $x=0.05$, and $x=0.08$ of Ca concentration[15–18] several features have been established. (i) Bragg peaks, at low temperature, indicate a mean canted antiferromagnetic state. (ii) Diffuse scattering is observed, indicating ferromagnetic inhomogeneities of characteristic size, distributed in a quasiliquid order. These inhomogeneities have been attributed to hole-rich regions, embedded in a hole-poor medium. (iii) The spin dynamics, where high-energy and low-energy spin-wave branches are observed, reflects both the mean antiferromagnetic canted state and the inhomogeneous features. The high-energy spin wave can be described by a Heisenberg Hamiltonian with two nearest-neighbor couplings, characteristic of the *A*-layered antiferromagnetic structure, as in pure $LaMnO_3$. The low-energy spin-wave branch is characteristic of an isotropic ferromagnetic coupling. The q dependence of its susceptibility reveals a tight connection with the ferromagnetic inhomogeneities. So, the Ca-doped compounds, at low values of doping, exhibit both homogeneous and inhomogeneous magnetic features. The same observations have been found in a Sr-doped compound,[19] showing the general character of these observations in low-doped manganites.

In this paper we present a neutron-scattering study at three concentrations, 0.1, 0.125, and 0.2, allowing a general survey of the concentration range where the system, still an insulator, approaches the metallic state. The phase diagram, established in the $0 \leqslant x \leqslant 0.2$ range, is pecularly studied in the $0.125 \leqslant x \leqslant 0.2$ range, where, below the ferromagnetic transition temperature, a structural transition appears. The spin dynamics is determined along the two relevant q directions for the *A*-type structure, [110] and [001]. In the $x=0.10$ compound, which exhibits many features similar to the $0<x<0.1$ ones, we observe a strong anisotropy in the q dependence of the low-energy spin-wave intensity that we relate to a two-dimensional character for the static ferromagnetic clusters. At $x=0.125$, *an abrupt change* occurs. We no more observe a modulation in the diffuse scattering, suggesting a percolation of the ferromagnetic clusters. Moreover, one spin wave branch, anisotropic, is detected, with an anomaly at some $q_0=(1.25,1.25,0)$. At $x=0.2$, the spin-wave dispersion appears as isotropic. Whereas the most intense excitations allow us to define the dispersion curve of a usual ferromagnet with an anomaly at q_0 as for $x=0.125$, additional magnetic excitations are observed at larger q, forming an optical branch. They reveal a more complex magnetic state, suggesting a high sensitivity of the magnons to an

underlying structural periodicity.

The paper is organized as follows. Experimental details are given below, in this introduction. The structural and magnetic phase diagram for the $0 \leqslant x \leqslant 0.2$ concentration range is presented in Sec. II. Diffuse-scattering experiments obtained for $x=0.05$, 0.08, 0.1, and 0.125 are reported in Sec. III. The spin dynamics observed for $x=0.1$, 0.125, and 0.2 is described in Sec. IV and, finally, Sec. V is devoted to a discussion and conclusion.

Single crystals of $La_{0.9}Ca_{0.1}MnO_3$ were grown by a floating-zone method associated with an image furnace at the Laboratoire de Physico-Chimie de l'état Solide in Orsay, France, with a volume of about 0.4 cm^3. Samples with higher Ca concentrations were grown by the same method at the MISIS Institute of Moscow, with similar volumes. Preliminary results are also reported for $x=0.17$. The mosaicity of these samples is small: 0.6°, 0.5°, and 0.5° for the $x=0.1$, 0.125, 0.17, and 0.2 doped compounds, respectively. The Ca concentration has been checked by comparing the lattice parameters with the previous determination of Matsumoto[20] and, for $x=0.125$ and $x=0.17$, by performing surface microscopy. A good agreement is also found with the phase diagram of Cheong, published in Ref. 21, except for the sample with nominal concentration $x=0.2$, which rather corresponds to $x=0.19$. Nevertheless, in the following we keep the nominal concentration x=0.2. All our samples are twinned in three space directions, but for $x=0.1$, 0.125, and 0.17, the orthorhombicity is large enough to allow the resolution of the Bragg peaks corresponding to different domains.

Neutron-scattering experiments were performed on several triple axis spectrometers installed either on thermal or cold neutron sources at the Orphée reactor of Laboratoire Léon Brillouin (1T, 4F1, 4F2, G43) and at the reactor of Institut Laue-Langevin (IN14). Elastic spectra have been obtained using a wave vector of $k_i=k_f=1.55$ Å^{-1} associated with a berylium filter and tight 10′-10′ collimations. Energy spectra were measured using various fixed outcoming wave vectors k_f (from 2.662 to 1.05 Å^{-1}) and pyrolytic graphite or berylium as a filter. All the samples were oriented with a horizontal (001,110) scattering plane, defined in $Pbnm$ symmetry ($c/\sqrt{2}<a<b$) except for the $x=0.2$ single crystal, which was studied in all q directions.

Macroscopic magnetization measurements were performed at Laboratoire de Physico-Chimie de l'état Solide in Orsay and at the SPEC (CEA-Saclay) with a superconducting quantum interference device magnetometer, for fields up to 5 T.

II. STRUCTURAL AND MAGNETIC PHASE DIAGRAM

Structural and magnetic transition temperatures have been determined from Bragg-peak intensities using elastic neutron scattering and are reported in Fig. 1.

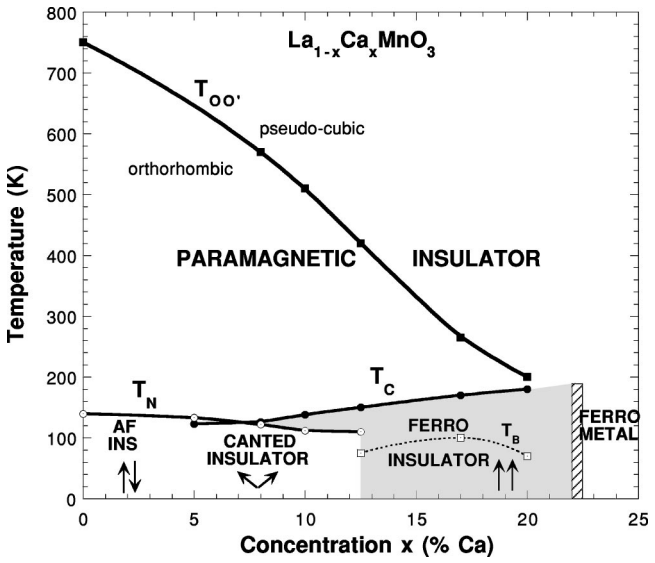

FIG. 1. (T,x) phase diagram of $La_{1-x}Ca_xMnO_3$, determined by neutron-scattering measurements on single crystals.

A. Structural transition

In Fig. 1, the solid line through the filled squares can be identified as the Jahn-Teller transition temperature $T_{OO'}$. There, the system evolves from a pseudocubic phase with a dynamical Jahn-Teller effect to an orthorhombic $Pbnm$ phase with a cooperative and static Jahn-Teller effect. We observe a strong decrease of the structural transition temperature from $T_{OO'}=750$ K in pure $LaMnO_3$ (Ref. 22) to $T_{OO'}=200$ K at $x=0.2$. Actually, $T_{OO'}$ has been determined from the increase of the q linewidth, which locates the temperature where a single Bragg peak in the O phase splits into two in the O' phase due to twinning. For $x<0.2$, the experimental q resolution allows a determination of the cell parameters in the orthorhombic phase, as shown in Fig. 2(a) and Fig. 2(b) for $x=0.1$ and $x=0.125$, respectively. For $x=0.2$, the Bragg peaks are not resolved whatever the temperature in the O' phase located below 200 K. At $x \geqslant 0.125$, a further decrease of the orthorhombicity is observed below 100 K, indicating a reentrance for the high-temperature pseudocubic phase. We call T_B the temperature of the inflexion point of this variation. Very interestingly, a similar anomaly has been observed in Sr-doped samples.[12,13,23,24] In $La_{0.875}Sr_{0.125}MnO_3$, where T_B is called $T_{O'O''}$, this variation has been shown to correspond to a rapid change in two of the three Mn-O distances.[13] Although the same evolution is expected for these Ca-doped samples, such a structural study is lacking. Moreover, in Sr-doped compounds, new Bragg reflections occur below $T=T_{O'O''}$, namely, at $(0,0,2l+1)$, which are forbidden in $Pbnm$ symmetry, and at $(0,0,l+0.5)$.[12,13,25] They have been related either to a polaron ordering[25] or to an orbital ordering.[14] In the present study, nuclear $(0,0,2l+1)$ peaks are actually detected at $x=0.2$ only, in the whole studied temperature range ($10 \text{ K} \leqslant T \leqslant 300$ K) without any temperature anomaly, whereas the superstructures $(0,0,l+0.5)$ have not been found in the present study, being likely short range or dynamic.

B. Magnetic structure

As reported in Fig. 1, below $T_{OO'}$, two magnetic transitions are observed. *For* $x=0.1$, a ferromagnetic transition

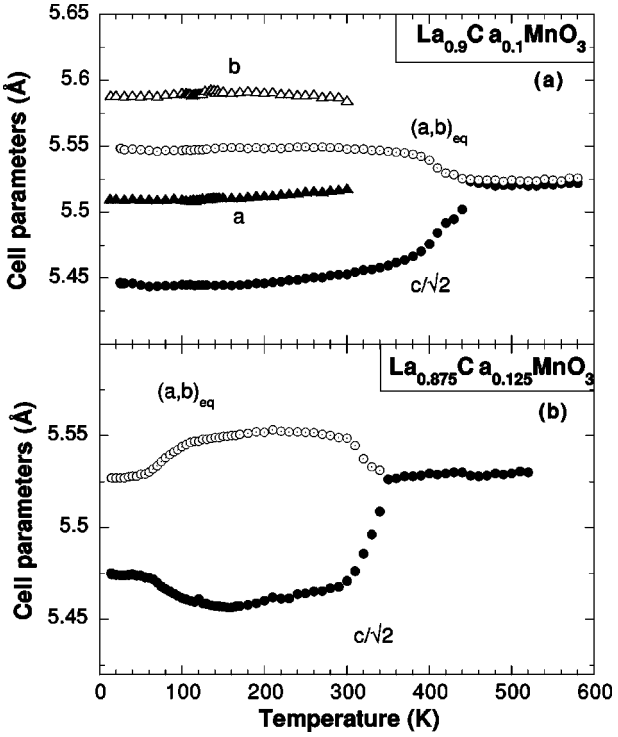

FIG. 2. Cell parameters versus temperature (a) $x=0.1$ and (b) $x=0.125$. $(a,b)_{\mathrm{eq}}$ is deduced from the (110) Bragg-peak position and defined by $(a,b)_{\mathrm{eq}}=\sqrt{2}/\sqrt{1/a^2+1/b^2}$.

occurs at $T_C=138$ K, and an antiferromagnetic ordering of spin components occurs at $T_{CA}=112$ K. This succession of phases has been predicted by de Gennes[3] for some value of the parameters of the mean-field model. Interestingly, the direction of the ferromagnetic spin component shows a complex evolution with temperature, reflected in the $\tau=(001)$, (002), (020), and (200) Bragg-peak intensities reported in Figs. 3(a), 3(b), and 3(c), respectively. In the neutron cross section, the geometrical factor implies that only spin components perpendicular to **Q** can contribute to the scattering intensity. Therefore, between T_C and T_{CA}, the observation of a constant intensity for the (020) Bragg peak [Fig. 3(c)] indicates that spins are aligned along the **b** axis. At T_{CA}, Rietveld refinements indicate that an antiferromagnetic component develops also along **b**, keeping the A_y-type structure found for $x<0.1$. The concomitant decrease of the (002) Bragg-peak intensity [Fig. 3(b)] reflects a rotation of the ferromagnetic spin component from the **b** to **c** axis, as antiferromagnetism develops. This effect was not observed at $x=0.08$, where T_C and T_{CA} are very close to each other, and the ferromagnetic spin component is along **c** at all temperatures. Therefore, at low temperature, the *mean* spin components deduced from Bragg peaks consist of an antiferromagnetic component along the **b** axis, a ferromagnetic one along the **c** axis, and another small ferromagnetic component along the **a** axis. From this spin configuration, we define a *mean* canting angle (angle between the spin direction and the direction **b** of the antiferromagnetism) equal to $\theta_c=\arccos(\sin\theta\sin\phi)=61.5°\pm5°$.

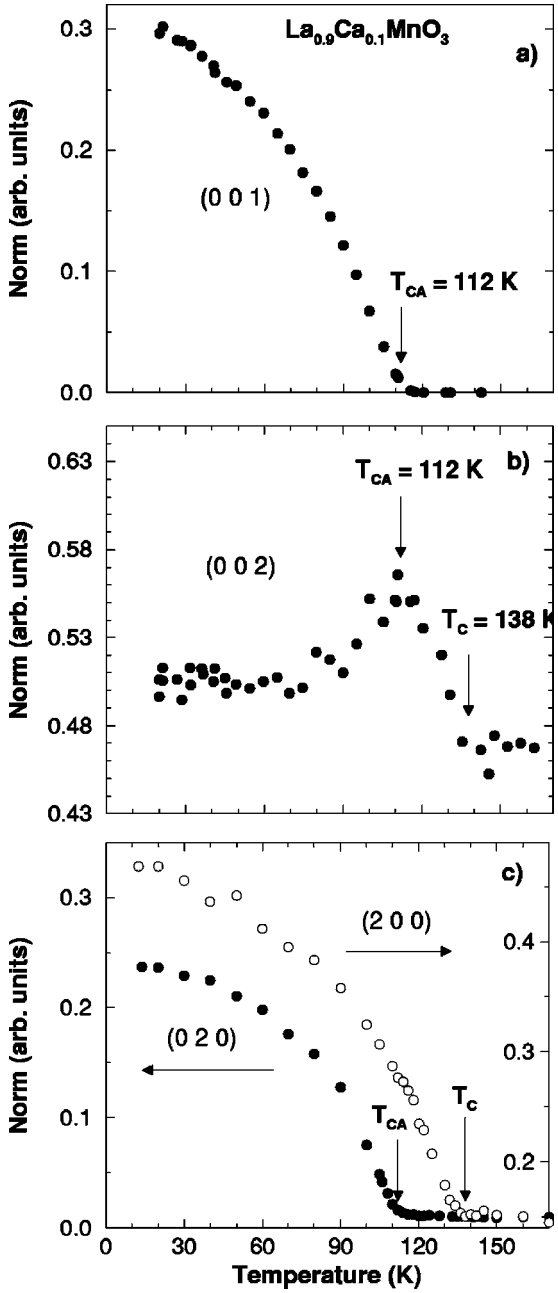

FIG. 3. $La_{0.9}Ca_{0.1}MnO_3$. Integrated intensities versus temperature (a) of (001), (b) (002), and (c) (020) (filled circles) and (200) (open circles) Bragg peaks.

The concentration dependence of the canting angle θ_c deduced from observations in the $0<x\leqslant0.1$ range is reported in Fig. 4. A strong jump of θ_c is observed between $x=0.08$ and 0.1. This abrupt increase of the ferromagnetic component is correlated with its rotation in the (**c**,**a**) plane. This fast evolution beyond $x=0.08$ departs from the smooth cosine law predicted by de Gennes.[3]

At $x=0.125$, $T_C=155$ K. Below 110 K, a very small increase of the $(0,0,2l+1)$ Bragg peaks indicates the occurrence of a small antiferromagnetic spin component or a residual canting in this sample. Resistivity measurements performed on this sample indicate a small decrease just below

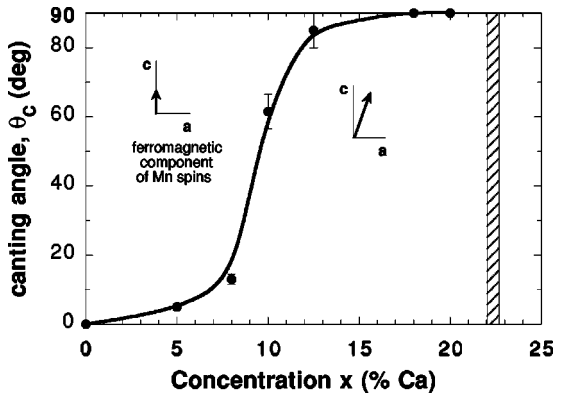

FIG. 4. Evolution of the canting angle with doping. The full line is a guide for the eye.

T_C, with an upturn below 110 K where this compound becomes insulating.[26] Finally, we mention an anomalous increase in the temperature variation of some magnetic Bragg peaks at the temperature called $T_B \approx 80$ K [see the (112) Bragg intensity in Fig. 5], concomitant with the structural transition temperature $T_{O'O''}$ [cf. Fig. 2(b)].

At $x=0.2$, T_C is determined at 185 K (Fig. 6). No increase of intensity is detected in the temperature variation of the odd-integer $(0,0,2l+1)$ Bragg peaks, so that this compound is fully ferromagnetic. The resistivity exhibits a downturn at T_C but it still increases at lower temperature.[26] Our results agree with previous publications, where the metal/insulator transition at T_C has been observed at $x_{Ca} \approx 0.22$,[27,28] as indicated by the hatched area in the phase diagram (Fig. 1).

As found for $x=0.125$, a marked increase of some nuclear and ferromagnetic Bragg-peak intensity (110) or (002), which are unresolved, is also observed at lower temperature, below $T_B=75$ K. Actually, its amplitude depends on the rate of cooling. At 50 K, measurements of the Bragg peak (002) have been repeated during several hours. The intensity of the peak and its position are found to fluctuate between two close points (Fig. 6). This behavior is typical of an instability or a metastability with both magnetic and structural character. Preliminary measurements at $x=0.17$, where the resolution is sufficient to detect the structural transition at $T_B = T_{O'O''} = 100$ K, reveal a similar anomaly.

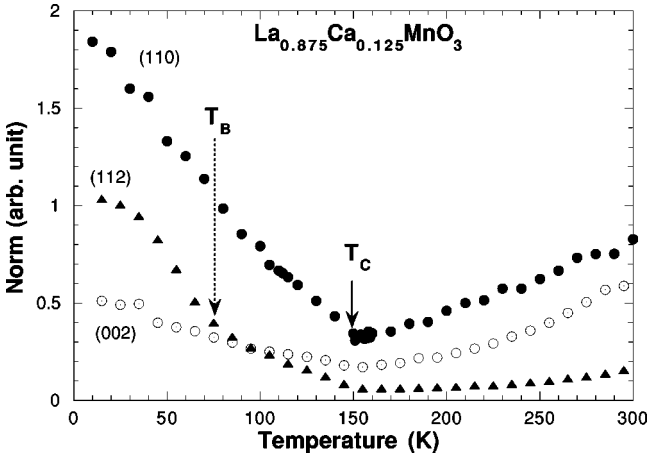

FIG. 5. $La_{0.875}Ca_{0.125}MnO_3$. Integrated intensities of (110), (112), and (002) Bragg reflections versus temperature.

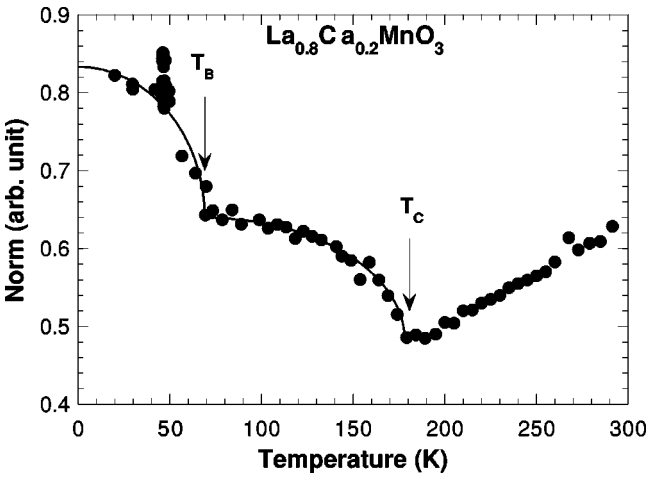

FIG. 6. $La_{0.8}Ca_{0.2}MnO_3$. Integrated intensity of (110) or (002) Bragg peaks versus temperature. At 50 K, the various points roughly determine two distinct values, observed as a function of time (see the text).

In conclusion, a transition line $T_B(x)$ is defined for $x > 0.1$ as reported in Fig. 1. It corresponds to a "reentrant" structural transition where the orthorhombicity is reduced. This line is qualitatively similar to that observed in Sr-substituted samples[29] around $x=0.125$, except that the corresponding temperatures are larger in this latter case. Qualitative differences also appear in the temperature behavior of the $(0,0,2l+1)$ Bragg peaks, which exist at all temperatures in Ca-substituted samples. Moreover, the superstructures of the type $\mathbf{Q}=(0,0,l+0.5)$, which occur below $T_{O'O''}$ in Sr-substituted samples,[25] have not been studied enough in the Ca-substituted ones for a clear conclusion. A more extensive structural study of the Ca-doped samples is planned for a complete characterization.

C. Magnetization measurements

Magnetization measurements have been performed as a function of temperature under a 100-Oe applied field and at 10 K under large magnetic fields. Small slabs, cut from the four single crystals with $x=0.05$, 0.08, 0.1, and 0.125 have been studied. The demagnetizing field, similar in all samples, has been minimized by allowing a free alignment of the slab along the field. Fits of magnetization with a Curie-Weiss law $\chi = C/(T-\Theta_P)$ show that $\Theta_P(x)$ strongly increases with x and merges into $T_C(x)$ at $x=0.125$. The same variation with x was found in a previous study.[20]

Zero-field magnetization can be obtained by extrapolation of the high-field measurements to $H=0$, assuming that the volume consists of one domain (Fig. 7). At $x=0.05$ and 0.08, a quantitative agreement is found with the variation of the canting angle reported in Fig. 4. At $x=0.1$ the magnetization is smaller than expected from the canting angle, which could be explained by an inaccurate determination of the volume due to twinning.

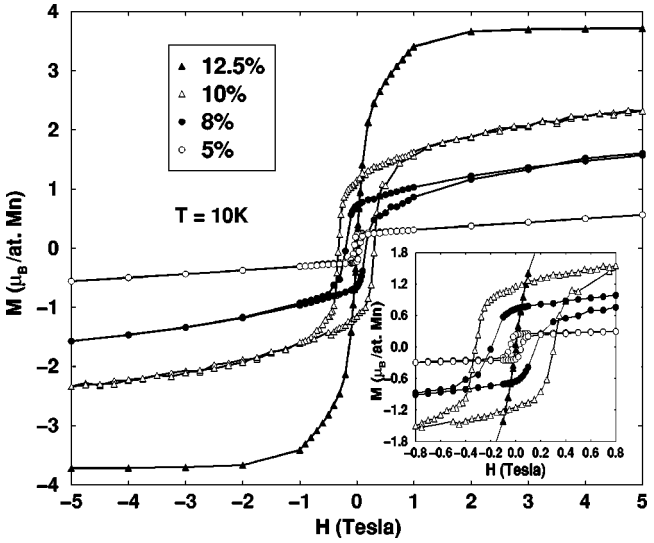

FIG. 7. Magnetic-field dependence of magnetization at $T=10$ K for $La_{1-x}Ca_xMnO_3$; $x=0.05$, 0.08, 0.1, and 0.125. Inset: same measurements displayed for small field values.

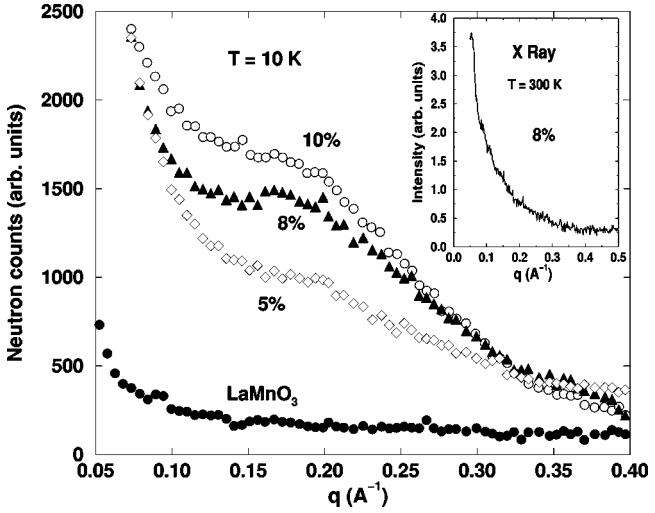

FIG. 8. Small-angle neutron-scattering (SANS) spectra measured with a XY multidetector along the [110] direction at $T=10$ K for $La_{1-x}Ca_xMnO_3$; $x=0$, 0.05, 0.08, and 0.1. Inset: small-angle x-ray measurements at room temperature for $x=0.08$.

An interesting evolution of the coercive field as a function of x is observed, as shown in Fig. 7 and its inset. The coercive field first increases from pure $LaMnO_3$ up to $x=0.1$ and reduces to a very small value at $x=0.125$. Similar observations were found in Sr-doped samples.[30,31]

Such a hysteresis cycle indicates a pinning of the magnetic domains to the lattice, which increases up to $x=0.1$ and disappears at $x=0.125$. A relation of this evolution with the growth of ferromagnetic clusters, expected to percolate at $x=0.125$ where the antiferromagnetism disappears (cf. the next section), is suggested.

III. MAGNETIC DIFFUSE SCATTERING

For $x=0.08$, a diffuse scattering, characteristic of short range ferromagnetic correlations, has been already reported.[17] In this section, we present the evolution of this diffuse scattering with the Ca concentration in the $0<x\leqslant 0.125$ range, using two neutron techniques: one, with no energy analysis but a XY multidetector, and the other one, with an energy analysis.

A. Small-angle scattering with no energy analysis

Small-angle neutron-scattering (SANS) experiments, using a XY multidetector, have been carried out on samples with $x=0$, 0.05, 0.08, and 0.1 calcium concentrations at several temperatures. The twinned samples were oriented so that the scattering plane is defined by the [110] and [001] directions. Spectra collected in all directions of this scattering plane with the multidetector indicate that the intensity is nearly isotropic. This allows us to check that the various twinned domains have equal volumes. In Fig. 8, intensities, corrected for sample transmissions, are compared for several doping rates at $T=10$ K and along the [110] direction. A strong evolution is observed between pure $LaMnO_3$ on the one hand, showing a low and nearly q-independent signal, and the doped samples on the other hand, characterized by a growing q-dependent modulation. This modulation is typical of a characteristic distance between similar ferromagnetic clusters. Interestingly, the same experiment using x-ray scattering and a linear multidetector does not show any modulation (see the inset of Fig. 8 at $x=0.08$ and $T=300$ K). Since x-ray scattering provides a good contrast between La and Ca ions, we are sure of the absence of any chemical clustering of Ca impurities in the same q range within these samples.

This modulation lies upon a steeply q-decreasing intensity which could be assigned to nuclear scattering (dislocations). In this diffraction experiment with no energy analysis, the determination of this parasitic contribution at high temperature cannot be subtracted due to the contamination of the paramagnetic excitations. Only the large q range, attributed to purely magnetic scattering, can be analyzed. A fit with a Gaussian function, $I(q)\propto\exp(-q^2R^2)$, indicates an increase of ferromagnetic correlation length from $2R=14$ to 17 and to 19 Å for x varying at 0.05, 0.08, and 0.1, respectively. This is shown in Fig. 9, where $\ln(I)$ versus q^2 has been reported. We conclude that the ferromagnetic clusters are small and grow very slowly with x.

B. Small-angle scattering with energy analysis

In order to analyze the magnetic scattering in the whole q range, elastic diffuse-scattering measurements ($\omega=0$) have been performed using a three-axis spectrometer. The $15\leqslant T\leqslant 300$ K range has been studied along several q directions, using $k_i=1.25$ Å^{-1}. Intensities have been put on an absolute scale, using a vanadium sample and a transmission correction. The temperature-independent scattering observed above T_C (nuclear contribution) could be subtracted from the low temperature scattering, determining the magnetic contribution. This magnetic signal is reported in Fig. 10(a) for $x=0.05$ and 0.08 and Fig. 10(b) for $x=0.1$ and 0.125 at $T=15$ K. Starting from $x=0.05$, the intensity of the modula-

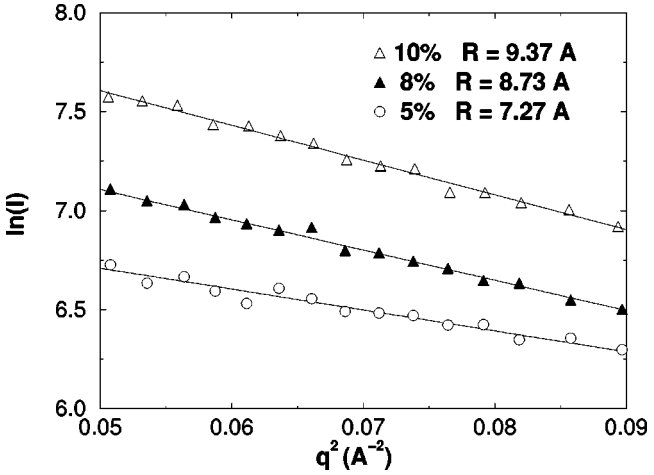

FIG. 9. Fits of $\ln(I)$ versus q^2 obtained in the large q range of the SANS spectra for $La_{1-x}Ca_xMnO_3$, $x=0.05$, 0.08, and 0.1.

tion rapidly increases up to $x=0.08$ with a shift of q, at maximum intensity, towards larger values. Then, at $x=0.1$, the intensity stays approximately at the same value, with a broadening of the modulation indicating additional intensity at smaller q. At $x=0.125$, we no longer observe any modulation but the intensity is much larger at very small q and a flat q dependence is observed at large q.

A detailed analysis of the $x=0.08$ sample has been previously reported.[17] In the picture where the q modulation results from a characteristic distance between small ''ferromagnetic'' clusters, the intensity can be expressed as

$$I(q) \propto |\Delta m^z|^2 N_V V^2 |F(qR)|^2 J(q), \tag{1}$$

where $F(qR)$ is the form factor of one cluster, and $J(q)$ is a function that characterizes the correlations in the spatial distribution of the clusters (assimilated to a liquid distribution function). The density N_V and the volume V are defined from the q dependence of $I(q)$ through the $J(q)$ and $F(qR)$ functions. Such a model is based upon two assumptions: (i) The diffuse-scattering intensity arises from the $\langle S_i^z S_j^z \rangle$ spin correlations with $Oz//\mathbf{c}$. This assumption was actually checked in a previous study on an $x=0.06$ Sr-doped sample, thanks to the absence of twinning.[19] The ''magnetic'' contrast $|\Delta m^z|$ is defined as the difference between the average magnetizations m^z inside and outside the cluster. (ii) The cluster picture is isotropic (spherical shape and isotropic cluster distribution in all directions). This latter assumption was found to be inaccurate in the twin-free $x=0.06$ Sr-doped sample. Instead, a picture of *anisotropic* platelets, with a size within the ferromagnetic layers about three times larger than perpendicular to them, could be determined. In the present case, Eq. (1) provides a semiquantitative analysis with the three parameters of the model: the size $(2R)$, the mean distance d_m, and a minimal distance of approach $d_{\min}$. The dot-dashed lines in Fig. 10(a) are the best fit of the data in this model. The cluster size varies very slowly with x, from 14 Å for $x=0.05$ to 17 Å for $x=0.08$. In this approach, the magnetic

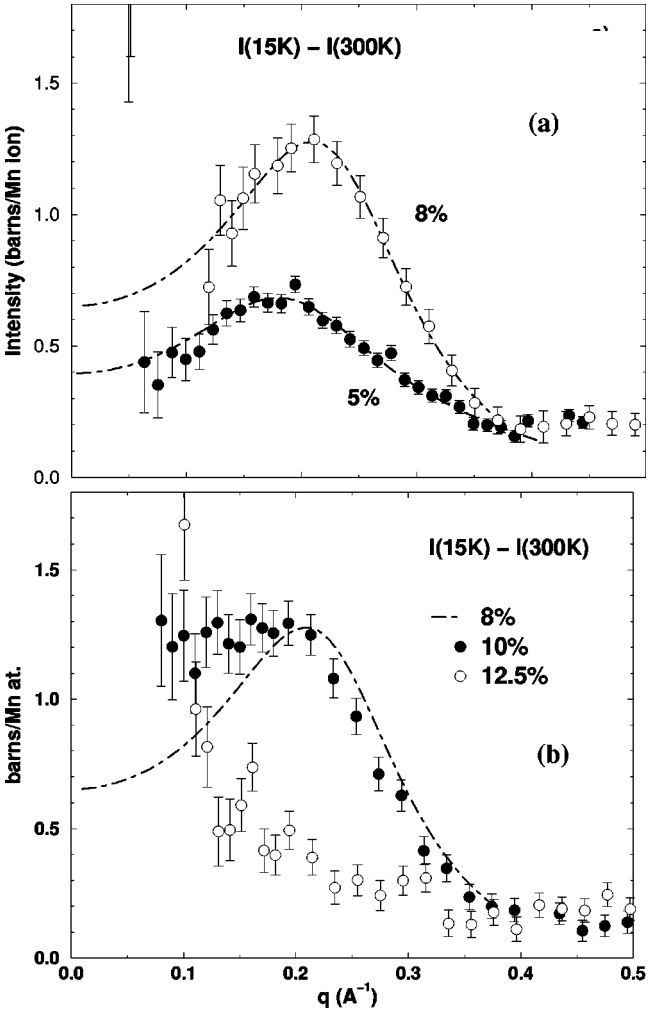

FIG. 10. Magnetic scattering observed at a small angle in $La_{1-x}Ca_xMnO_3$; (a) $x=0.05$ and 0.08 and (b) $x=0.1$ and 0.15.

intensity is mainly proportional to the square of the cluster volume V and to the square of the magnetic contrast Δm^z. Therefore, the increase of the diffuse scattering by a factor of ≈ 2 between $x=0.05$ to $x=0.08$ is mainly taken into account by the increase of the cluster size from 14 Å to 17 Å, with a magnetic contrast of $\Delta m^z \approx 0.7 \mu_B$. This is a small contrast, indicating a rather smooth picture. Of course, the assumption of isotropy leads to an overestimation of the volume or an *underestimation* of Δm^z. We note that the volume ratio between the clusters observed at $x=0.05$ and at $x=0.08$ roughly compares with the corresponding ratio of the hole concentrations.

At $x=0.1$, the evolution is different from that between 0.05 and 0.08. An additional scattering intensity is observed indicating new ferromagnetic correlations on a scale larger than the intercluster distance. Therefore, the evolution between $x=0.08$ and 0.1 can be characterized in terms of a coalescence of clusters, rather than in terms of a size variation, as it is for the evolution between $x=0.05$ and 0.08.

At $x=0.125$, $I(q)$ shows a strongly increasing intensity at very small q, whereas a flat q dependence persists at large q.

This signal cannot be characterized further. This evolution is likely related to the occurrence of the percolation of the ferromagnetic inhomogeneities.

At $x=0.2$, a diffuse scattering of nuclear origin is observed around (2.5,2,0) that is $(0.25,2.25,0)_{cub}$ and equivalent points in reciprocal space in the cubic indexation. This is in perfect agreement with previous observations reported in Ca-doped samples.[32,33] Since this nuclear diffuse scattering indicating a short-range polaron ordering along the [100] direction cannot be related to the spin correlations described above (static) and below (dynamic), it is not described further.

The temperature dependence of the magnetic diffuse scattering observed at $x \leqslant 0.1$ has been reported previously[17] showing that the intensity disappears around the temperature for the magnetic transition T_C.

The existence of ferromagnetic clusters could be the consequence of the polarization by a single mobile hole as previously predicted.[7] However, in the present case, the comparison between the cluster density and the hole density rather indicates that one ferromagnetic cluster contains several holes. In our first article,[17] using the assumption of an isotropic model (same distance between clusters whatever the q direction), we have deduced a density of clusters $\approx 1/60$ times smaller than that of the holes. The anisotropy discovered in the $I(q)$ function of a twin-free Sr-doped sample indicates that this value has been overestimated by at least a factor of 2. Anyway, this very aproximative evaluation confirms the picture of a charge segregation with hole-rich regions embedded in a Mn^{3+} hole-poor network.

In conclusion, we get a picture of ''ferromagnetic'' clusters with a diameter of about 16 Å, in repulsive interaction, which grow very slightly and start to coalesce at $x=0.1$. They are observable as far as the long-range antiferromagnetic order exists ($0<x<0.125$). The observation of a characteristic distance between the clusters, as well as the observation of a ferromagnetic Bragg peak, requires that the mean magnetization inside each cluster is parallel to the same direction (here the **c** axis). This leads to a modulated canted state picture instead of a true phase separation.

As shown below, the study of the spin dynamics will corroborate and specify this picture.

IV. SPIN DYNAMICS

In Sec. IV A, spin dynamics of the $x=0.1$ compound and in Sec. IV B spin dynamics of $x=0.125$ and $x=0.20$ are reported along the two [001] and [110] directions of the *A*-type magnetic structure. In Sec. IV C, the evolution with x of the parameters determined from the spin dynamics is displayed.

A. $x=0.1$: The approach to the ferromagnetic transition

1. Low-temperature spin dynamics: Comparison with $x<0.1$

a. The high-energy branch. As recalled in the introduction, in this low-doped regime, two spin-wave dispersion curves are observed, characterized as high-energy and low-energy branches. For the high-energy branch, the assignment of a dispersion to the [001] or the [110] direction is unambiguous, in spite of twinning, because of the two distinct periodicities in the reciprocal space. Examples of spectra obtained along the $[00\zeta]$ direction, which determines the antiferromagnetic coupling, are reported in Fig. 11 up to the antiferromagnetic zone boundary.

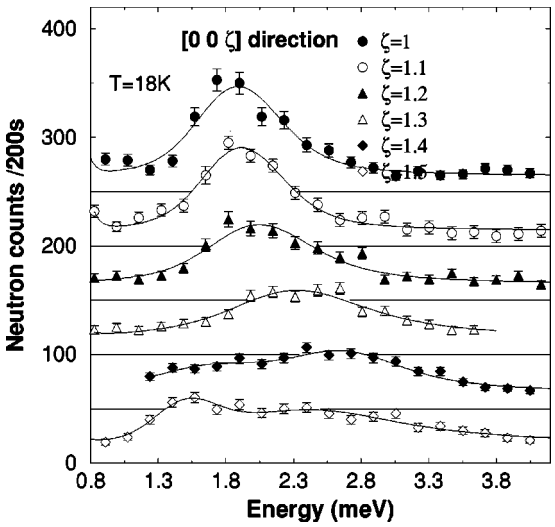

FIG. 11. Energy spectra measured in the $[00\zeta]$ direction up to the antiferromagnetic zone boundary, at $T=18$ K. Fits correspond to calculated intensities using Lorentzian functions convoluted with the spectrometer resolution.

At $\mathbf{Q}=\tau=(0,0,1)$, a large gap value, $\Omega_0=1.86$ meV at $T=18K$, is obtained. By increasing $\mathbf{q}$ along [001] ($\mathbf{q}=\mathbf{Q}-\tau$), the energy very weakly disperses as the intensity decreases whereas the damping, roughly twice larger than in the undoped case, moderately increases. The energy saturates when approaching the zone boundary $\mathbf{Q}=(0,0,1.5)$ and a lower-energy mode belonging to the low-energy spin-wave branch is observed. This high-energy branch has also been measured along the direction of propagation [110] starting from (110), which defines the ferromagnetic coupling. There, only spin waves with Q beyond (1.1,1.1,0) have a measurable intensity. Therefore, the small q range along this direction has been studied starting from the antiferromagnetic Bragg peak (111). The dispersion curve of this high energy branch is reported in Fig. 12 by empty triangles along the two symmetry directions. A fit of the dispersion using a Heisenberg model with four first in-plane neighbor couplings J_1, ferromagnetic and J_2, antiferromagnetic, along [001], and with an effective single-ion anisotropy C (Refs. 15, 16 and 18) is also shown by a continuous line in Fig. 12. On the same figure, results obtained for $x<0.1$ and $x=0$ are also reported for comparison. The variation of J_1 and J_2 with doping is displayed in Fig. 13. It reveals a linear variation for the two effective couplings, showing the weakening of J_2 and the strengthening of J_1. This linear variation $J_2(x)$ agrees pretty well with $J_2=0$ at $x=0.125$, where the antiferromagnetic Bragg peak (001) disappears.

As a remarkable result, the gap Ω_0 of this spin-wave branch keeps the same value for all x (see Fig. 12 and Fig. 14). This value is also the same, within our experimental

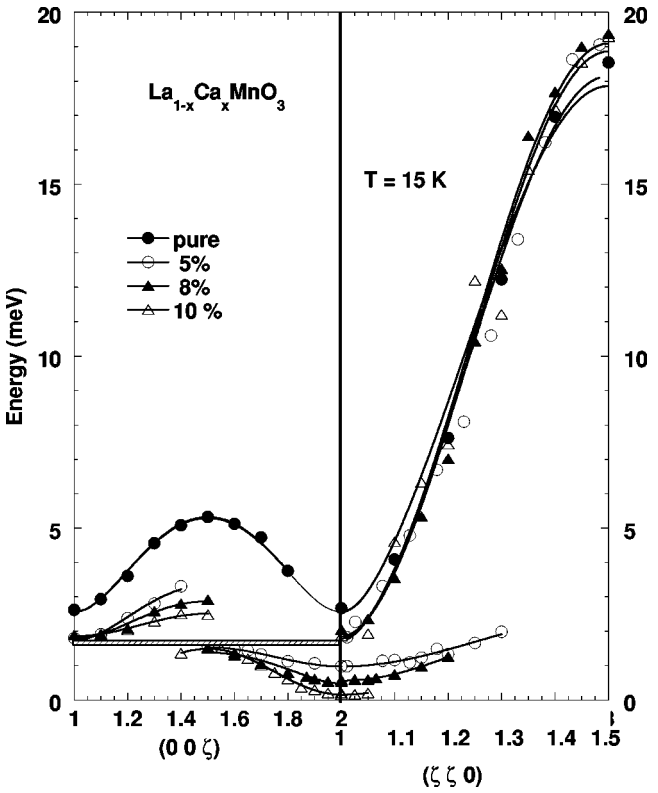

FIG. 12. Dispersion curves along $[00\zeta]$ from (001) to (002) Bragg peaks (left panel) and along $[\zeta\zeta 0]$ from (110) to (1.5,1.5,0) (right panel) for $x=0$, 0.05, 0.08 and 0.1 compounds. At $x=0.1$, along $[\zeta\zeta 0]$, only the small q excitations of the low-energy spin-wave branch (empty triangle) have measurable intensity. The solid lines are fits (see the text).

accuracy, as that measured in Sr-doped samples,[19,34] also reported in Fig. 14.

b. The low-energy branch. For the case of the low-energy branch, the assignment to the [110] or [001] directions is more difficult, since the periodicities in the q space are the same along the two directions (ferromagnetic character). It

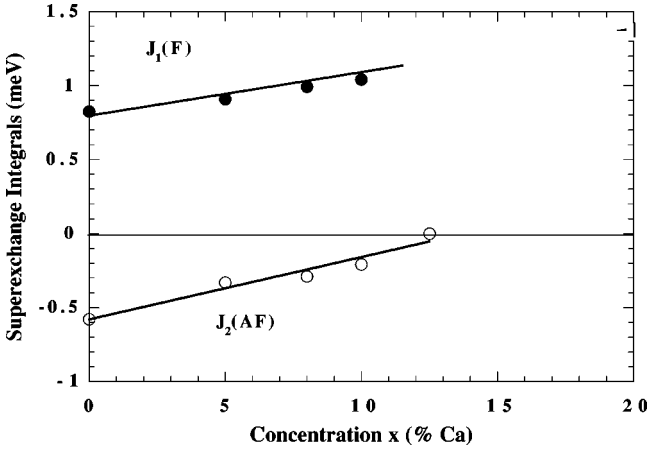

FIG. 13. Ferromagnetic coupling J_1 and antiferromagnetic coupling J_2, associated with a superexchange type of coupling (see the text) as a function of Ca concentration.

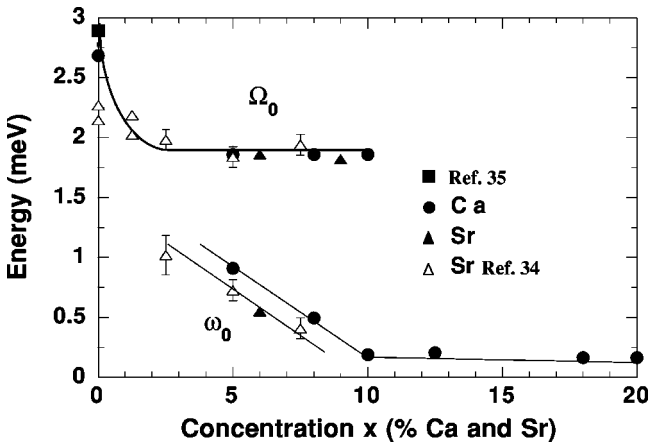

FIG. 14. Energy gaps corresponding to the two types of spin-wave branches, versus Ca and Sr concentrations. Filled symbols: using the neutron technique (Refs. 15, 17 and 19) at $T=15$ K and (Ref. 35) at $T=8$ K. Open symbols: Using the antiferromagnetic resonance technique (Ref. 34) at $T<20$ K.

can be solved, however, as long as the orthorhombicity of the structure is measurable. In $q//\tau$ experiments, where the Bragg peaks (002) and (110) are a center of symmetry for $\omega(q)$, the assignment is made by performing $+q$ and $-q$ measurements. If the center of symmetry is (002) [resp. (110)], the q direction is [001] (resp. [110]). As shown in Fig. 15, all the $+q$ and $-q$ magnons lie on a symmetric curve with respect to $q=0$, in the case where the (002) Bragg peak is chosen as the q origin.

Examples of energy spectra are shown in Fig. 16, with the energy-integrated intensity $S(q)$ reported in the inset. Therefore, the new feature, at this concentration, comes from the fact that spin waves propagating along [110] cannot be mea-

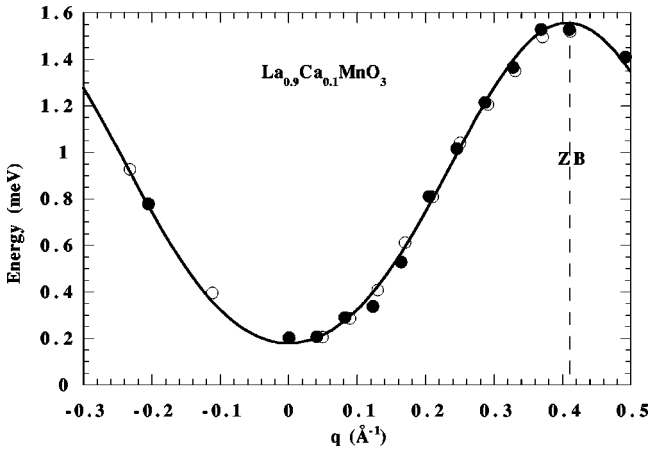

FIG. 15. Filled and empty circles correspond to energy excitations of the low-energy spin-wave branch measured in two perpendicular q directions, attributed to [110] and [001], respectively, for one domain. The two corresponding dispersions coincide if the q origin is the (002) Bragg peak whatever the domain. $(+q)$ and $(-q)$ measurements are symmetric with respect to the (002) Bragg peak (see the text). At this $x=0.1$ concentration, the (002) and (110) Bragg-peaks positions are distant from 0.031 Å^{-1}.

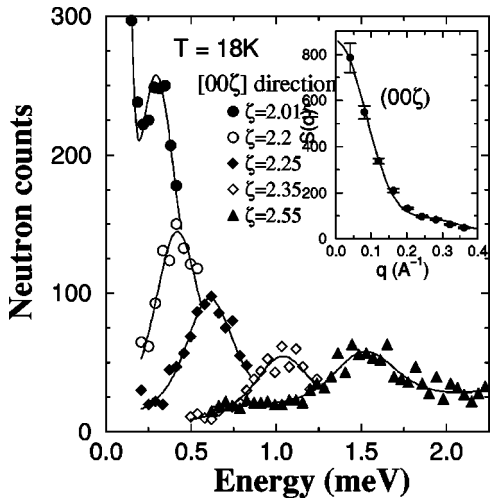

FIG. 16. Energy spectra of the low-energy magnetic excitation along $[0,0,\zeta]$. The energy-integrated intensity $S(q)$ of this spin-wave branch is shown in the inset.

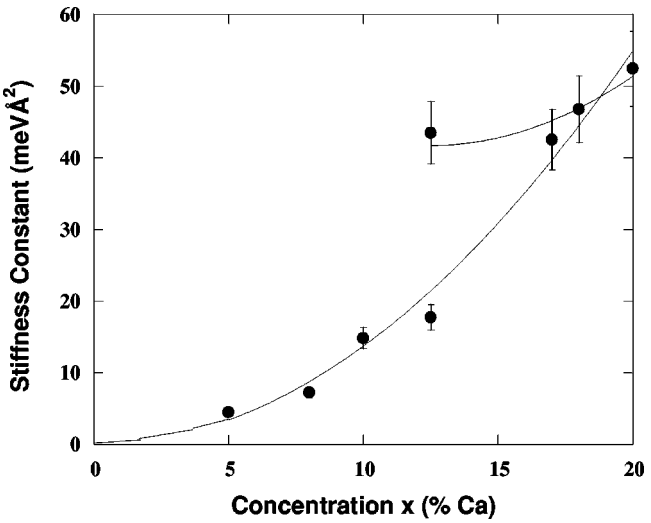

FIG. 17. Stiffness constant determined from the low-energy spin-wave branch versus Ca concentration. The values at $x=0.17$ and 0.18 are deduced from a preliminary study.

sured. Only propagation along [001] is clearly observed up to the antiferromagnetic zone boundary (cf. Fig. 15). The difficulty in measuring a dispersion curve along [110] means that the intensity of the corresponding excitations, superimposed to those propagating along [001], exhibits a very fast decrease with increasing q. Such a strong anisotropy of the spin-wave intensity has already been observed in a Sr-doped sample, where, in the absence of twinning, both directions could be unambiguously identified.[19] Thanks to a quantitative correspondence between the correlation lengths deduced from the static and dynamic spin correlations, the relation with the anisotropic shape of the static clusters has been clearly established. In the same way, we can relate the anisotropy of the spin-wave intensity $S(q)$, in this $x=0.1$ sample, to the anisotropy of the shape of the static clusters, hidden here because of twinning (cf. Sec. III). Within this picture, the q profile of the spin-wave intensity $S(q)$ [$S(q)$ is proportional to the susceptibility], reported in the inset of Fig. 16, with two distinct q dependencies, can be interpreted as the superposition of the intensities of the spin wave propagating along both [110] and [001], characterized by a steep and a slow q dependence, respectively. The fit of $S(q)$ with a sum of two Lorentzian functions gives two correlation lengths: $\zeta=17$ Å and $\zeta=5$ Å. This anisotropy is very similar to the anisotropy of the spin-wave intensity observed in the twin-free Sr-substituted sample, which, in this latter case, could be quantitatively compared to the anisotropy of the cluster size.[19]

The whole q range of $\omega(q)$ along [001] can be fitted by a cosine law, and the small q range, by a $\omega=Dq^2+\omega_0$ law as in our previous studies. The fitted dispersion is reported in Fig. 12 with experimental data and compared with the $x=0.05$ and 0.08 cases. Values of ω_0 and D are reported in Fig. 14 and Fig. 17, respectively, showing the decrease of ω_0 and the increase of D with x.

The comparison of the low-energy spin-wave branches reported for $x=0.05$, 0.08, and 0.1 in Fig. 12 reveals that, along [001] where intensity is measurable whatever x, all the dispersion curves bend at the zone boundary $\mathbf{Q}=(0,0,1.5)$ or $q_0=(0,0,.5)$ with the *same* energy value $\omega(q_0)\approx 1.57$ meV. This observation is the counterpart of the other remarkable observation concerning the x-independent gap Ω_0 of the high-energy branch, pointed out above, in the description of the high-energy branch (cf. Fig. 18). Both features reveal strongly nonlinear effects with x.

The two spin dynamics are tightly coupled. Along [001] they spread into two adjacent energy ranges, defining a small forbidden energy region (hatched area in Fig. 12). As previously emphasized, they correspond to *two types of excitations of a single magnetic ground state*.

2. Temperature dependence of spin waves

The phase diagram reported in Fig. 1 has pointed out the existence of ferromagnetic and insulating phases between $T_C=138$ K and $T_{CA}=112$ K, with a spin direction along **b** at T_C rotating towards **c** below T_{CA}, where the antiferromagnetic long range order occurs. The temperature evolution of

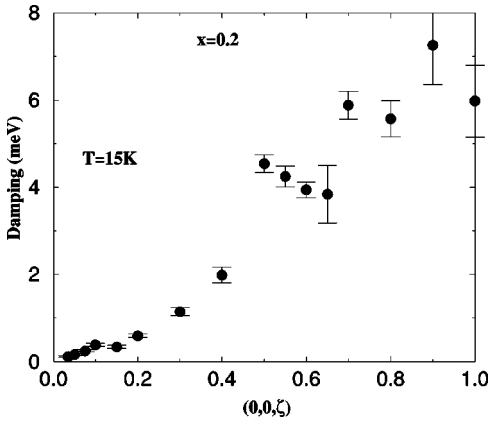

FIG. 18. Damping versus q of the magnetic excitation measured at $x=0.2$ along [001] or [110].

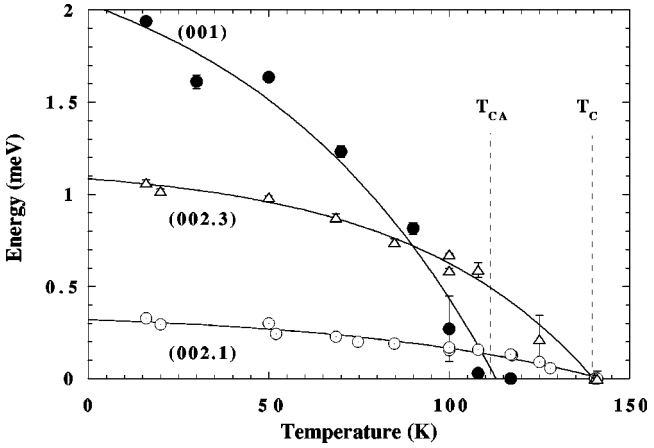

FIG. 19. Temperature dependence of some magnetic excitation energies. The full circles correspond to the gap measured at (001). Empty circles correspond to excitations of the low-energy spin-wave branch measured at (002.1) and (002.3). The solid lines are guides for the eye.

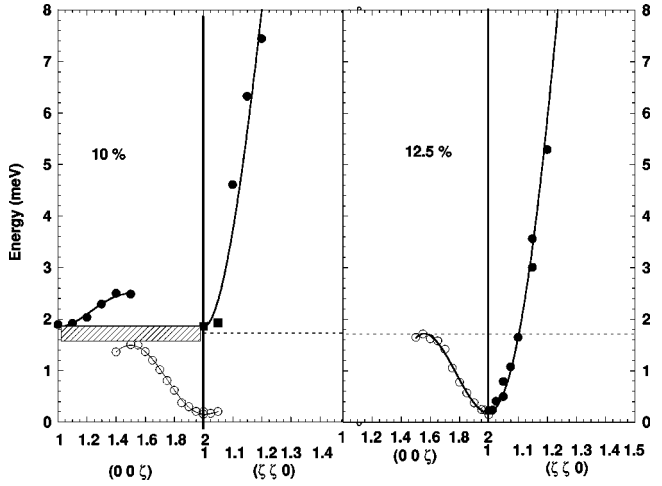

FIG. 20. Comparison of the dispersion curves measured along the $[00\zeta]$ and $[\zeta\zeta 0]$ directions in $x=0.1$ (left panel) and $x=0.125$ (right panel). The two squared symbols in the left panel recall that these excitations have been obtained around (111) instead of (110), where they have no intensity. Continuous lines: see the text.

the spin dynamics provides the opportunity to probe more deeply this ferromagnetic state. The temperature evolution of the gap characteristic of the high-energy branch, measured at the antiferromagnetic Bragg peak $\tau=(001)$, is shown by filled circles in Fig. 19. It reveals a softening of this mode with a complete renormalization at T_{CA}. Above T_{CA}, we still observe antiferromagnetic (AF) quasielastic spin fluctuations (energy spectra centered at $\omega=0$). By contrast, the magnetic excitations of the low-energy spin-wave branch measured close to the ferromagnetic Bragg peak (002) are still well defined at T_{CA} and are fully renormalized at T_C, without any anomaly at T_{CA}. This is shown in the same figure, where the temperature evolution of two modes, at $q=(002.1)$ and (002.3), are reported by open circles and triangles, respectively. We conclude that the occurrence of the long-range ferromagnetic order at T_C is driven by the ferromagnetic coupling revealed by the low-energy branch only.

B. $x=0.125$ and $x=0.2$: The ferromagnetic and insulating phases

The concentrations $x=0.125$ and $x=0.2$ correspond to the ferromagnetic and insulating states. Their spin dynamics, at low temperature, is described successively.

1. $x=0.125$

The spin-wave dispersions $\omega(q)$ for q along [001] and [110] are reported in the right panel of Fig. 20, and in Fig. 21. The assignment of a dispersion curve to the [001] direction of propagation is unambiguous, in spite of twinning, and uses the same arguments as for $x=0.1$ (cf. Fig. 15). The assignment of the other dispersion curve to the [110] direction is the consequence of the first deduction.

The main result is the observation of one spin wave branch, within the exerpimental accuracy, as expected for a ferromagnetic state. The excitations defining the AF superexchange coupling along [001] at $x<0.125$ are not observed. This is what one could expect from the linear variation of $J_2(x)$, where $J_2\approx 0$ at this concentration (Fig. 13). This spin-wave branch exhibits the same gap as that of the low-energy spin-wave branch in the canted state described above. Therefore, a continuity between $x<0.125$ and $x=0.125$ is observed for the spin dynamics through the low-energy branch. This observation rules out the idea of a two-dimensional magnetic state at the disappearance of the antiferromagnetism, which could be suggested when missing the low-energy spin-wave branch.[35] The dispersion curve differs strongly along [001] and [110] and exhibits some anomaly in both directions at $\mathbf{q}_0=[(0,0,1.5)$ or $(1.25,1.25,0)]$ as described below.

Along [001], the dispersion curve is very similar to the low-energy spin-wave branch for $x<0.125$. It bends with avanishing intensity at $\mathbf{q}_0=(0,0,0.5)$, the zone boundary of the antiferromagnetic state, reaching the same x-independent value defined for $x<0.125$ (see the horizontal dotted line in

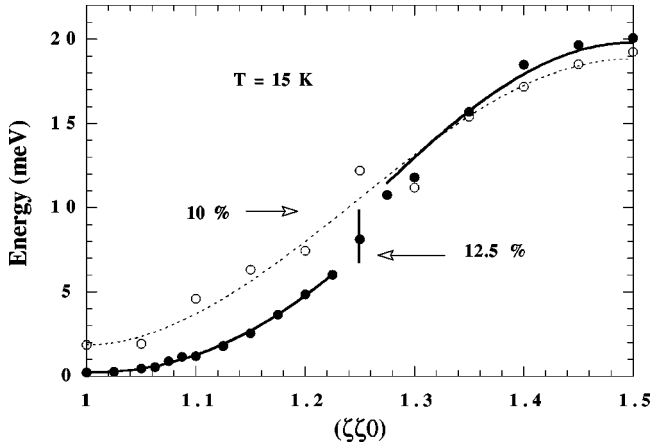

FIG. 21. Spin-wave dispersion along [110] for $x=0.125$ (full circles) and $x=0.1$ (empty circles).

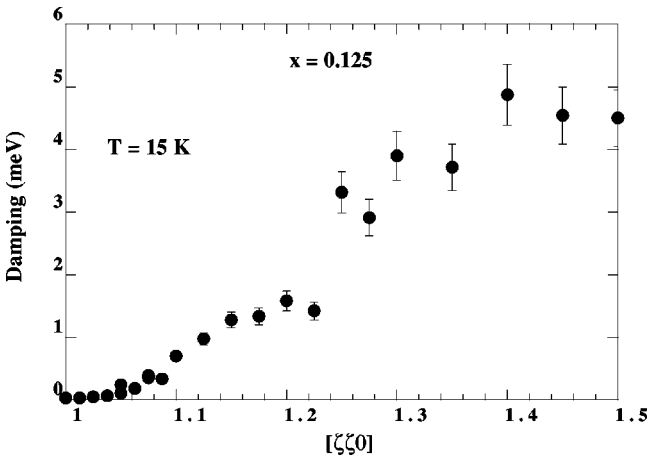

FIG. 22. q dependence of the magnon energy linewidth or damping along [110] for $x=0.125$.

Fig. 20). In spite of the disappearance of the antiferromagnetic coupling, the similarity with $x<0.125$ in the dynamic susceptibility implies the persistence of some feature, related to the vicinity of the canted state. In the canted state, we have outlined the tight connection between the dynamic susceptibility of the low-energy spin-wave branch and the static correlations defining the ferromagnetic clusters, attributed to a charge segregation. At $x=0.125$, this persisting spin dynamic feature may reflect a persisting charge segregation along [001]. The gap value and the stiffness constant determined from a fit $\omega=\omega_0+Dq^2$ are reported in Figs. 14 and 17, respectively.

Along [110], $\omega(q)$ can be measured up to the ferromagnetic zone boundary (1.5,1.5,0) as shown in Fig. 21. The dispersion differs from that observed at $x<0.125$ especially at small q where only a spin-wave dispersion with a small

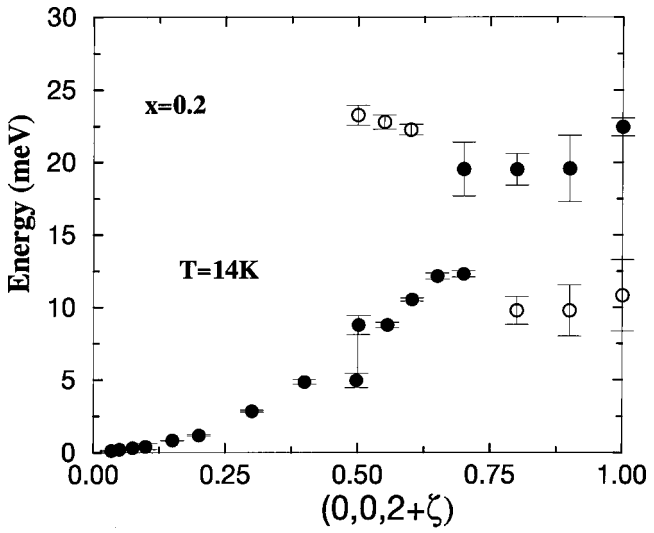

FIG. 23. Spin-wave dispersions determined at $x=0.2$ for q along the [110] or [001] directions using the orthorhombic unit cell (edge of the small perovskite cube). The continuous line is a guide for the eye. The splitting into two modes at $\mathbf{q}_0=(0,0,2.5)$ is suggested by the jump in the energy linewidth at this $\mathbf{q}$ value, reported in Fig. 21.

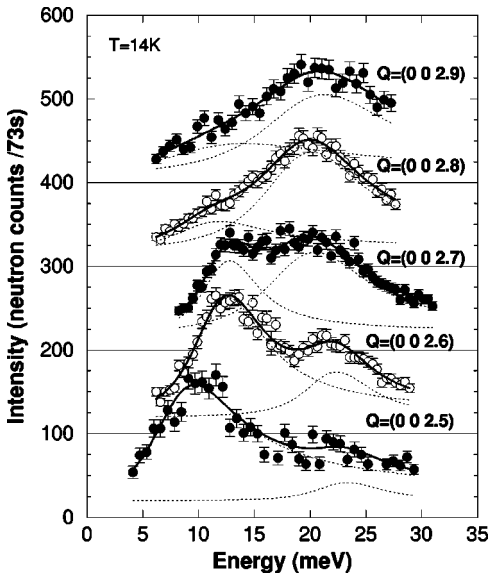

FIG. 24. Energy spectra measured at $x=0.2$ along [110] or [001], showing two modes for each q value. The dashed lines correspond to a fit with two Lorentzian functions convoluted with the spectrometer resolution.

gap value is detected, within the experimental accuracy (see comparison with $x=0.1$ in Fig. 21). This strong change at small q suggests that, unlike the [001] direction, ferromagnetic platelets have percolated within the ferromagnetic layers, in agreement with the observation of a strongly increasing intensity in diffuse scattering at very small q [Fig. 10(b)]. The whole dispersion cannot be fitted by a Heisenberg model with first-neighbor couplings only or a single cosine law, unlike the case of the high-energy branch at lower concentrations. Instead it exhibits an ''S'' shape, suggesting two different behaviors depending on the lower or larger q ranges considered. In addition, an anomaly appears at half the zone boundary $\mathbf{q}_0=(1.25,1.25,0)$ as seen in Fig. 21. This anomaly can be understood as a small splitting in the dispersion as suggested from the energy linewidth of these magnetic excitations, displayed in Fig. 22, where a discontinuity is observed at this $\mathbf{q}_0$ value.

We mention that a similar anomaly has been reported in $La_{0.85}Sr_{.15}MnO_3$,[23] at the same $\mathbf{q}_0$ value, indexed as (0,0,2.5), however, and related to the occurence of the new periodicity indicated by the odd-integer superlattice peaks $(0,0,2l+1)$. However, the present observations are thought to be related to the [110] direction only, instead of [001], so that it cannot be explained by these superlattice peaks. Additional excitations have been also observed at higher energy. This new feature is discussed below for $x=0.2$, where these excitations are more easily detected.

For $q<q_0$, a quadratic law for $\omega(q)$ determines a stiffness constant with a much larger value than along [001],outlining the anisotropic character of the ferromagnetic coupling at this critical concentration.

2. $La_{0.8}Ca_{0.2}MnO_3$

At $x=0.2$, where the transition $T_{OO'}$ occurs very close to T_C (cf. Fig. 1), the orthorhombicity is too small for the (110)

and the (002) Bragg peaks to be resolved, and odd-integer (0,0,2l+1) Bragg peaks are observed (cf. Sec. II A). However, for continuity with the $x<0.2$ concentration range, we still keep the $Pbnm$ indexation. The spin-wave dispersion obtained at 14 K is reported in Fig. 23 for the two superimposed [001] and [110] directions, corresponding to the $[100]_{cub}$ direction when indexed in the cubic cell.

At this concentration, we first notice the same anomaly at $\mathbf{q}_0=(0,0,2.5)$ or (1.25,1.25,0) in the q variation of the magnon energy linewidth (Fig. 18) as in the $x=0.125$ sample. As for $x=0.125$, the jump of the energy linewidth at this value suggests a splitting or a gap in the dispersion.

In addition, at $q\approx q_0$ and beyond, extra excitations are observed at higher energy (≈ 22 meV), forming an optical branch, with a growing intensity as q increases towards the zone boundary. Concomitantly, the intensity of the lower-energy excitation decreases. Corresponding energy spectra are shown in Fig. 24.

Excitations with the largest intensity allow to draw a ''main'' dispersion curve up to the zone boundary, which, unlike the $x=0.125$ concentration, appears identical for the [001] and [110] directions. This ''main'' spin-wave dispersion cannot be fitted with a Heisenberg model using first-neighbor coupling. As above, for $x=0.125$, the dispersion within the $q<q_0$ range has been fitted using a quadratic law, determining a stiffness constant, and gap values reported in Fig. 17 and Fig. 14, respectively.

C. Evolution of the dynamic parameters with x

We report the evolution with x of all the parameters defined from the spin dynamics.

1. Variation with x of the two energy gaps

In Fig. 14, the variation with x of the two gaps, the large one Ω_0, associated with the excitations of the A-type magnetic structure and of the small one ω_0, associated with the low-energy spin-wave branch, are displayed. In the same figure, measurements of both Ca- and Sr-doped samples obtained by neutron[15,16,19,17,35] (filled symbols) and by antiferromagnetic resonance[34] (empty symbols) are reported. Except for $x=0$ where a small discrepancy is observed between neutron data[35,15] and the AF resonance technique,[34] the agreement of the data is excellent, whatever the Ca-doped or the Sr-doped samples. Actually, the low-energy gap reported at $x=0$ by antiferromagnetic resonance,[34] unresolved by the neutron technique, cannot have the same meaning as ω_0, related to the low-energy branch, which appears only by doping.

Beyond the very small concentration range ($x\approx 0.02$) where the large gap Ω_0 decreases quickly, two regimes may be defined, the boundary being around the ferromagnetic transition. (i) In the AF canted state (namely, $x<0.125$ for the Ca substitution and $x<0.1$ for the Sr one), Ω_0 is found to be x independent. The same observation is found for the Sr-doped samples, showing the same constant energy value. As outlined in Sec. IV A 1, this observation is associated with the existence of a forbidden energy region (hatched area) separating the energy range of the two spin wave branches along [001] (cf. Fig. 12). These nonlinear features with x, observed both at $q=0$ and at $q\neq 0$, disagree with the usual picture of a mean-field canted state. At $q=0$, a monotonous decrease of the large anisotropy gap Ω_0, associated with the antiferromagnetic structure, is expected,[34] instead of an x-independent behavior. Moreover, in such a model, the two spin-wave branches would cross each other along [001] at $q=(0,0,1.5)$, instead of keeping in the separated energy range as shown in Fig. 12.

Concerning $\omega_0(x)$, it quickly decreases up to $x=0.1$, and very slowly beyond, in the ferromagnetic insulating state. $\omega_0(x)$ is shifted at larger x for Ca doping compared to the Sr one, in agreement with the experimental fact that Sr induces a stronger ferromagnetic character than Ca. In our inhomogeneous picture, the origin of $\omega_0(x)$ may be related to the size of the platelets. Therefore, the ferromagnetic spin component inside the platelet rotates more easily as the platelets' size increases with x.

2. Evolution of the stiffness constant D with x

In Fig. 17, we have reported the variation $D(x)$, obtained for seven single crystals ($x=0.05$, 0.08, 0.1, 0.125, 0.17, 0.18, and 0.2), deduced from a fit with a $\omega(q)=Dq^2+\omega_0$ along [110] or [001] in the small q range only. D reflects the long-range ferromagnetic coupling. It shows three regimes.

For $x<0.125$, the fit corresponds to the small q range of the lower-energy branch, which is isotropic. Since the corresponding spin-wave susceptibility reflects the anisotropic form factor of the ferromagnetic clusters (platelets), this isotropy could appear surprising. Actually, the stiffness constant D, which reflects the long-range ferromagnetic coupling, may involve the magnetic coupling inside the clusters (double exchange) and between the clusters through the canted magnetic state of the AF matrix, reflecting the fact that the local magnetizations inside the clusters are coupled through the matrix.

At $x=0.125$, where a single spin-wave branch is observed, the dispersion differs along [001] and [110]. The step increase observed along [110] corresponds to the collapse between the two spin-wave branches into a single one, whereas the low value of D along [001] is in perfect continuity with the evolution of the low-energy spin-wave branch. As discussed previously, the abrupt increase of this coupling along [110] and the absence of variation of this ferromagnetic coupling along [001] agree with a picture of *percolation of the platelets occurring in the ferromagnetic layers only*. This implies persisting inhomogeneous features along [001].

At $x=0.175$ and beyond, D appears isotropic within our accuracy level. Interestingly, the stiffness constant does not significantly vary between the value along [110] measured at $x=0.125$ and that, isotropic, found at $x=0.2$. Apart from this x range, a continuity of $D(x)$ between the smallest x values and $x=0.2$ can be suggested, when fitting the whole variation by a quadratic function of x.

3. Evolution of the ''effective'' superexchange constants with x

In Fig. 13, the ''effective'' superexchange couplings, ferromagnetic (J_1), and antiferromagnetic (J_2) deduced from

the high-energy branch along [110] and [001] directions, respectively, are reported up to $x=0.1$. A linear variation is observed with x. It yields $J_2 \approx 0$ close to $x=0.125$, in agreement with the observation of a single ferromagnetic spin-wave branch at this concentration (cf. above). The renormalization of superexchange coupling by hole doping agrees rather well with the model of Feiner and Oles.[36] However this model does not take into account charge segregation and therefore cannot predict another spin-wave branch. Therefore, it would lead to a two-dimensional (2D) ferromagnetic behavior at $x=0.125$ where $J_2=0$. By contrast, we show the continuous increase of the three-dimensional ferromagnetic coupling with x, revealed by the ferromagnetic low-energy branch. At $x \geqslant 0.125$, where several anomalies are observed in the spin-wave dispersion, the ''effective'' superexchange couplings can no longer be defined.

V. CONCLUSION

The three studied concentrations $x=0.1$, 0.125, and 0.2, described in this paper, characterize three distinct steps in the evolution of the magnetic ground state towards the insulator-metal transition. The $x=0.1$ sample exhibits the same original properties reported in the very low-doping regime ($x=0.05$ and 0.08), i.e., an additional spin-wave branch of ferromagnetic character and a static diffuse scattering, characteristic of ferromagnetic inhomogeneities in interaction. The observation here is the strongly anisotropic q dependence of the intensity of the low-energy spin-wave branch. This may be related to the 2D character of the ferromagnetic clusters or platelets. This feature, readily observed in the diffuse scattering of a free-twin Sr-doped sample,[19] is difficult to observe in the static diffuse scattering reported here because of the twinning. These 2D ferromagnetic clusters are embedded in an average canted state. The proposed analysis of the diffuse scattering, which yields a density of clusters smaller than the density of holes, suggests a charge segregation. This charge segregation picture differs from the phase-separation picture, with antiferromagnetic and ferromagnetic states, predicted by the theory.[4–9] The fact that the ferromagnetic components inside the clusters point towards the same direction instead of pointing up or down at random implies the role of an additional coupling in the system not accounted for by usual theories. Dipole-dipole interaction between magnetic polarons has been previously suggested as a possible origin for this coupling.[37] We outline the unusual q dependencies of the spin waves along [001], showing two distinct types of excitations in a separated energy range, which strongly differs from what is expected for a canted state.[3] Instead, they agree with the inhomogeneous picture of ferromagnetic clusters coupled through the matrix.

The $x=0.125$ sample is the limit corresponding to the disappearance of the A-type antiferromagnetic structure. This ferromagnetic state results from two evolutions with x, occuring concomitantly: a linear decrease of the antiferromagnetic coupling analyzed in terms of an effective superexchange type, J_2 where $J_2 \approx 0$ at $x=0.125$ (homogeneous process) and, as revealed by the diffuse scattering, the growth of the ferromagnetic clusters, suggesting a kind of percolation of the hole-rich clusters at this concentration (inhomogeneous process). This magnetic percolation does not coincide with the percolation for transport properties (metallic state), since an insulating behavior is still observed at low temperature. At this concentration, one spin wave branch is detected within the experimental accuracy, as expected for a ferromagnet, but with an anisotropic dispersion. From the inhomogeneous picture derived at smaller concentration, this anisotropy could be explained by the percolation of the platelets occuring in the basal plane only (2D percolation). Such a 2D percolation has been actually predicted using a band model for $LaMnO_3$.[38] Whatever the true picture, this anisotropy implies some persisting inhomogeneous features along [001]. In addition, an anomaly is observed along [110] at q_0 in the spin-wave dispersion, corresponding to half the zone boundary.

In the $x=0.2$ sample, the spin-wave dispersion is isotropic within our accuracy. The anomaly observed at q_0, as for $x=0.125$, is now assigned to the two superimposed [001] and [110] directions. In addition, a magnetic optical branch is observed at larger q and larger energies. This feature could suggest that the magnon excitations are interacting with other excitations, magnetic or not. A physical process of magnon-phonon coupling has been suggested by Furukawa[39] in these systems. Other authors[40,41] have proposed a coupling between magnon and orbital excitations to explain the anomalous softening of magnons observed in the metallic state.[42] The study of the spin dynamics with temperature, especially below T_B where a reentrant structural transition is observed, will be important for a deeper understanding of this complex magnetic state. It will be reported in a forthcoming paper.

ACKNOWLEDGMENTS

The authors are very indebted to L. Noirez from Laboratoire Leon Brillouin for his help during the small-angle neutron experiments and A. Wildes from Institut Laue-Langevin (Grenoble). They further acknowledge M. Viret, B. B. van Aken, T. T. M. Palstra, A. Moreo, D. I. Khomskii, E. L. Nagaev, and A. M. Oles for stimulating discussions.

[1] E. D. Wollan and W. C. Koelher, Phys. Rev. **100**, 545 (1955).
[2] J. Goodenough, Phys. Rev. **100**, 564 (1955).
[3] P. G. de Gennes, Phys. Rev. **118**, 141 (1960).
[4] D. P. Arovas and F. Guinea, Phys. Rev. B **58**, 9150 (1998).
[5] D. I. Khomskii and G. A. Sawatzky, Solid State Commun. **102**, 87 (1997).
[6] M. Kagan, D. Khomskii, and M. Mostovoy, Eur. Phys. J. B **12**, 217 (1999).
[7] E. L. Nagaev, Phys. Status Solidi B **186**, 9 (1994); Phys. Rev. B **60**, 455 (1999).
[8] J. Riera, K. Hallberg, and E. Dagotto, Phys. Rev. Lett. **79**, 713 (1997).

[9] S. Yunoki, J. Hu, A. L. Malvezzi, A. Moreo, N. Furakawa, and E. Dagotto, Phys. Rev. Lett. **80**, 845 (1998).
[10] A. J. Millis, B. I. Shraiman, and R. Mueller, Phys. Rev. Lett. **77**, 175 (1996).
[11] H. Roder, J. Zang, and A. R. Bishop, Phys. Rev. Lett. **76**, 1356 (1996).
[12] H. Kawano, R. Kajimoto, M. Kubota, and H. Yoshizawa, Phys. Rev. B **53**, R14 709 (1996).
[13] L. Pinsard, J. Rodrìguez-Carvajal, A. H. Moudden, A. Anane, A. Revcolevschi, and C. Dupas, Physica B **234-236**, 856 (1997).
[14] Y. Endoh, K. Hirota, S. Ishihara, S. Okamoto, Y. Murakami, A. Nishizawa, T. Fukuda, H. Kimura, H. Nojiri, K. Kaneko, and S. Maekawa, Phys. Rev. Lett. **82**, 4328 (1999).
[15] F. Moussa, M. Hennion, J. Rodríguez-Carvajal, H. Moudden, L. Pinsard, and A. Revcolevschi, Phys. Rev. B **54**, 15 149 (1996).
[16] M. Hennion, F. Moussa, J. Rodríguez-Carvajal, L. Pinsard, and A. Revcolevschi, Phys. Rev. B **56**, R497 (1997).
[17] M. Hennion, F. Moussa, G. Biotteau, J. Rodríguez-Carvajal, L. Pinsard, and A. Revcolevschi, Phys. Rev. Lett. **81**, 1957 (1998).
[18] F. Moussa, M. Hennion, J. Rodríguez-Carvajal, L. Pinsard, and A. Revcolevschi, Phys. Rev. B **60**, 12 299 (1999).
[19] M. Hennion, F. Moussa, G. Biotteau, J. Rodríguez-Carvajal, L. Pinsard, and A. Revcolevschi, Phys. Rev. B **61**, 9513 (2000).
[20] G. Matsumoto, J. Phys. Soc. Jpn. **29**, 606 (1970).
[21] A. J. Millis, Nature (London) **392**, 147 (1998).
[22] J. Rodríguez-Carvajal, M. Hennion, F. Moussa, A. H. Moudden, L. Pinsard, and A. Revcolevschi, Phys. Rev. B **57**, R3189 (1998).
[23] L. Vasiliu-Doloc, J. W. Lynn, A. H. Moudden, A. M. de Leon-Guevara, and A. Revcolevschi, Phys. Rev. B **58**, 14 913 (1998).
[24] V. E. Arkhipov, V. S. Gaviko, A. V. Korolyov, V. E. Naish, V. V. Marchenkov, Y. M. Mukovskii, S. G. Karabashev, D. A. Shulyatev, and A. A. Arsenov, J. Magn. Magn. Mater. **196-197**, 539 (1999).
[25] Y. Yamada, O. Hino, S. Nohdo, R. Kanao, T. Inami, and S. Katano, Phys. Rev. Lett. **77**, 904 (1996).
[26] B. B. van Haken and T. T. M. Palstra (private communication).
[27] J. Dho, I. Kim, S. Lee, K. H. Kim, H. J. Lee, J. H. Lung, and T. W. Noh, Phys. Rev. B **59**, 492 (1999).
[28] N. N. Loshkareva, Y. P. Sukhorukov, S. V. Naumov, N. I. Solin, I. B. Smolyak, and E. V. Panfilova, Pis'ma Zh. Éksp. Teor. Fiz. **68**, 89 (1998) [JETP Lett. **68**, 97 (1998)].
[29] Y. Moritomo, A. Asamitsu, and Y. Tokura, Phys. Rev. B **56**, 12 190 (1997).
[30] M. Paraskevopoulos, J. Hemberger, A. Loidl, A. A. Mukhin, V. Y. Ivanov, and A. M. Balbashov, cond-mat/9812276 (unpublished) and cond-mat/9812305 (unpublished).
[31] Y. F. Popov, A. M. Kadomtseva, G. P. Vorob'ev, V. Y. Ivanov, A. A. Mukhin, A. K. Zvezdin, and A. M. Balbashov, J. Appl. Phys. **83**, 7160 (1998).
[32] Pengcheng Dai, J. A. Fernandez-Baca, N. Wakabayashi, E. W. Plummer, Y. Tomioka, and Y. Tokura, Phys. Rev. Lett. **85**, 2553 (2000).
[33] C. P. Adams, J. W. Lynn, Y. M. Mukovskii, A. A. Arsenov, and D. A. Shulyatev, Phys. Rev. Lett. **85**, 3954 (2000).
[34] A. A. Mukhin, V. Yu Ivanov, V. D. Travkin, A. Pimenov, A. Loidl, and A. M. Balbashov, Europhys. Lett. **49**, 514 (2000).
[35] K. Hirota, N. Kaneko, A. Nishizawa, Y. Endoh, M. C. Martin, and G. Shirane, Physica B **237–238**, 36 (1997).
[36] L. F. Feiner and A. M. Olés, Physica B **259–261**, 796 (1999).
[37] E. L. Nagaev, Fiz. Tverd. Tela (Leningrad) **13**, 891 (1971) [Solid State Ionics **13**, 738 (1971)].
[38] L. P. Gor'kov and V. Z. Kresin, Pis'ma Zh. Éksp. Teor. Fiz. **67**, 934 (1998) [JETP Lett. **67**, 985 (1998)].
[39] N. Furukawa, J. Phys. Soc. Jpn. **68**, 2522 (1999).
[40] G. Khaliulin and R. Kilian, Phys. Rev. B **61**, 3494 (2000).
[41] A. M. Oles and L. P. Feiner, *Orbital Order versus Orbital Liquid in Doped Manganites in Ground State and Finite Temperature Bandferromagnetism*, edited by K. Baberschke, M. Donath, M. Potthoff, and W. Nolting (Springer, New York, in press).
[42] Pengcheng Dai, H. Y. Hwang, Jiandi Zhang, J. A. Fernandez-Baca, S.-W. Cheong, C. Loc, Y. Tomioka, and Y. Tokura, Phys. Rev. B **61**, 9553 (2000).